



Impact of natural organic matter and inorganic solutes on energy recovery from five real salinity gradients using reverse electrodialysis



R.S. Kingsbury^a, F. Liu^{b,1}, S. Zhu^{a,1}, C. Boggs^{b,c}, M.D. Armstrong^a, D.F. Call^{b,*}, O. Coronell^{a,*}

^a Department of Environmental Sciences and Engineering, Gillings School of Global Public Health, The University of North Carolina at Chapel Hill, Chapel Hill, NC 27599, USA

^b Department of Civil, Construction, and Environmental Engineering, College of Engineering, North Carolina State University, Raleigh, NC 27695, USA

^c Department of Mechanical and Aerospace Engineering, College of Engineering, North Carolina State University, Raleigh, NC 27695, USA

ARTICLE INFO

Keywords:

Reverse electrodialysis
Salinity gradient energy
Ion exchange membranes
Natural organic matter
Blue energy

ABSTRACT

“Blue energy” technologies such as reverse electrodialysis (RED) have received significant research attention over the last several years as a means of generating clean electricity from natural salinity gradients (e.g., seawater and river water). To date, however, knowledge of RED is largely based on synthetic sodium chloride solutions that simulate natural waters. Accordingly, in this work we measured the RED performance of five real water pairs, including seawater, river water, desalination brine, saline wastewater from a pickling plant, and treated wastewater. We compared the performance of each real water pair with that of synthetic control waters to investigate the individual impacts of inorganic constituents (e.g., multivalent ions) and natural organic matter (NOM). Our results indicate that the presence of NOM has a larger impact on power density than ionic composition. Specifically, NOM reduced power densities by up to 43%, while inorganic constituents reduced power densities by up to 8% compared to control waters. Furthermore, UV-absorbing NOM present in the dilute compartment of the RED stack was strongly associated with reduced membrane permselectivity and energy efficiency. Taken together, our findings highlight the important role of organic matter in determining the RED performance of real waters.

1. Introduction

Reverse electrodialysis (RED) has received considerable attention in recent years as a means to generate sustainable electricity by mixing river water with seawater [1]. In certain regions with strong salinity gradients, RED could feasibly generate enough electricity to meet all local demand [2]. Nevertheless, RED systems operated with simulated seawater and river water continue to be challenged by low power densities ($1\text{--}2\text{ W m}^{-2}$) [1], which are not adequate to make coastal RED power plants feasible unless the cost of ion exchange membranes significantly decreases [3].

In addition to power generation from sea and river water, other RED applications are currently being investigated. Researchers have used RED to generate power from concentrated salt brines [4–8], to convert waste heat into electricity [9,10], and to store energy [11–14]. These alternative applications allow for the use of higher concentration gradients, which have been shown to improve power density substantially.

Despite their higher power densities compared to applications using seawater/river water salinity gradients, RED systems that use brines

have received comparatively little research attention. For example, of 42 experimental power densities reported in a recent review by Gi et al. [1], only three used concentration gradients significantly different from seawater/river water (e.g., $\sim 0.5\text{ M}$ and $\sim 0.01\text{ M NaCl}$). Moreover, real RED applications may involve waters containing natural organic matter (NOM) and salts other than sodium chloride, yet the vast majority of studies have been conducted using pure NaCl solutions. Several studies [5,7,15–24] have included other (e.g., multivalent) ions in the test solutions, and have observed negative impacts on performance compared to pure sodium chloride. In general, the presence of low concentrations of multivalent cations negatively impacts RED performance by reducing the membrane permselectivity and/or increasing membrane resistance [16,19,20,23–25]. Three studies [5,7,26] have compared the performance of real natural water pairs obtained in field conditions to that of comparable synthetic solutions, and found that the use of natural water pairs resulted in only 30–60% of the power density obtained from synthetic solutions. Three studies [21,22,27] explicitly considered the impact of NOM by feeding RED stacks with natural seawater and river water. Although the obtained power density was

* Corresponding authors.

E-mail addresses: dfcall@ncsu.edu (D.F. Call), coronell@unc.edu (O. Coronell).

¹ These authors contributed equally to the work.

initially about 80% of the theoretical expectation, it rapidly decreased due to membrane fouling. In two of these studies, the theoretical expectation was obtained from calculations based on open circuit voltage (OCV) and membrane resistance, as they did not test synthetic solutions for comparison. There have been several studies on the impact of NOM on electro dialysis (ED) performance [28–32]. However, since in ED the direction of ion transport is opposite and the range of current densities is generally higher than in RED, it is not clear whether findings from these ED studies are applicable to RED. Thus, a comprehensive understanding of the factors that contribute to lower power generation when using real waters compared to pure NaCl solutions is lacking.

Accordingly, the objectives of this work were to: (1) quantify the individual impact that ions other than Na^+ and Cl^- (hereafter referred to as “inorganic solutes”) and NOM in real waters have on RED performance relative to theoretical expectations; and (2) develop tools to evaluate the suitability of a given water pair for RED based on common water quality parameters. To achieve our objectives, we compared the performance of real waters with control waters of the same conductivity. The control waters contained either only the same ions present in the real waters (no NOM) or only NaCl. We selected pairs of real waters that occur in close physical proximity, and therefore represent potentially feasible scenarios for salinity gradient power extraction. The real water pairs comprised seawater/brackish water, seawater/rainwater, seawater/treated municipal wastewater, reverse osmosis (RO) brine/RO influent (i.e., brackish groundwater), and pickling brine/stormwater. For each water pair, we measured the power density, energy efficiency, OCV, and electrical resistance, and related these performance metrics to common water quality parameters.

2. Experimental

2.1. Real water pairs

We tested waters from five sites throughout the coastal regions of North Carolina, USA that represent potentially suitable sources for RED power extraction (Table 1). We also tested synthetic “seawater” and “river water” containing 30 g L^{-1} and 1 g L^{-1} NaCl, respectively, for comparison to the real water pairs.

The pH, temperature, and conductivity of each water were measured in the field using pH test strips and a handheld conductivity/temperature meter (Oakton Instruments, Vernon Hills, IL). Water samples were filtered on-site through $10 \mu\text{m}$ polypropylene felt filters (McMaster Carr, Atlanta, GA) to remove suspended particles, and immediately stored in headspace-free plastic containers. Samples were transported at ambient temperature (6–12 h of transportation time) and stored in a 4°C refrigerator upon returning to the laboratory. Waters were allowed to warm to room temperature ($\sim 20^\circ\text{C}$) prior to use.

2.2. Control water pairs

For each real water pair, we prepared two control water pairs to isolate the impacts of NOM and inorganic solutes on RED performance. The “multi-ion controls” simulated the major ionic composition of each real water, and lacked NOM. They were prepared from deionized water

Table 1

Water types investigated, their source locations, and abbreviations used throughout the manuscript.

Location	Water pair abbreviation	Concentrated water resource	Dilute water resource
Fishing pier/coastal facility	SW/RW	Seawater ^a	Rainwater collected in a cistern
Brackish estuary	SW/BW	Seawater ^a	Brackish surface water
Coastal wastewater treatment plant (WWTP)	SW/WW	Seawater ^a	Treated wastewater effluent
Reverse osmosis desalination plant	RO/GW	Reverse osmosis brine	Brackish groundwater (plant influent)
Pickling facility	PK/ST	Waste brine from pickling process	Stormwater collected on plant site
Synthetic water	NaCl/NaCl	30 g L^{-1} NaCl	1 g L^{-1} NaCl

^a All seawater was collected from a single location near the fishing pier, and is considered representative of seawater available at the other two locations along the North Carolina coast.

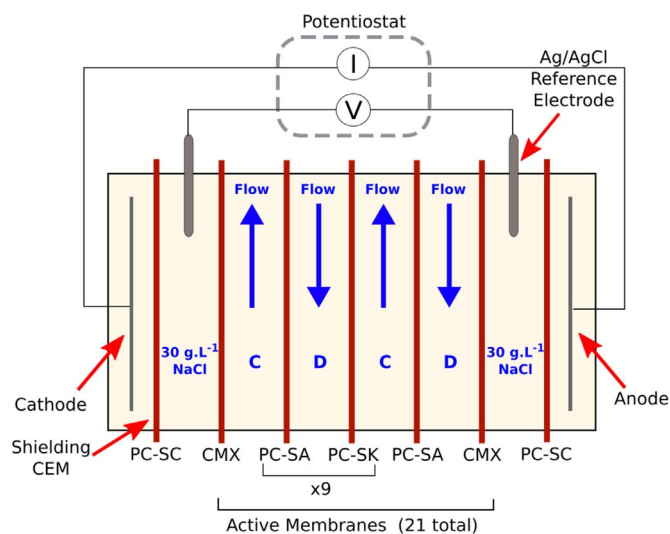


Fig. 1. Schematic of the RED stacks used in this work. Two identical stacks were outfitted with 10 pairs of ion exchange membranes (PC-SK and PC-SA, Neosepta CMX as outer membranes, for a total of 21 active membranes). Metal oxide coated titanium working electrodes were shielded from the membrane stack and the reference electrode compartments by 0.40 mm thick cation exchange membranes (PC-SC). C and D represent the concentrated and dilute feed waters, respectively, which flowed through the stack in counter-current configuration (as indicated by the blue arrows). Membrane active area = 64 cm^2 ; spacer thickness = 0.45 mm ; spacer open area $\approx 60\%$; crossflow velocity = 1 cm s^{-1} . (For interpretation of the references to color in this figure legend, the reader is referred to the web version of this article).

and granular salts in such a way that their conductivity, pH, and ionic composition matched the real waters (see Supplementary material). “NaCl controls” simulated the conductivity of each water, and contained only NaCl. NaCl control waters were prepared in analogous fashion to multi-ion controls by matching the measured conductivity of the real waters, but without adjusting pH.

2.3. Reverse electro dialysis stack

We tested all water pairs in two identical RED stacks (PCCell 64002, PCCell GmbH, Germany) outfitted with 10 pairs of ion exchange membranes (Fig. 1). Ag/AgCl reference electrodes (BaSi, Inc. RE-5B, West Lafayette, IN) were used to measure the electrical potential across the membrane stack. Separate feed solutions of 30 g L^{-1} NaCl were circulated in a closed loop through both the reference electrode compartments and the anode/cathode compartments, allowing current transfer to take place by electrolysis. We chose this electrode system for experimental convenience; a full-scale system would require an alternative electrode system (e.g. soluble redox couple, flow electrodes) to avoid generating hazardous gases (e.g., H_2 or Cl_2) at the electrodes [33,34]. All potential measurements reported in this work were recorded by the reference electrodes, meaning that the resistance of the electrode system (electrodes and redox reactions) and the shielding PC-SC membranes did not impact the measured stack resistance data. We chose this setup because in a scaled-up stack with 50 or more cell pairs,

the resistance of the electrode system would be negligible in comparison to that of the active membrane stack [4,35].

Since different water pairs were tested using two RED stacks, we developed a benchmarking procedure to confirm that the results from each stack were comparable to one another, and that the membranes did not deteriorate between testing the respective water pairs (see details in the [Supplementary material](#)). The benchmark resistance varied by less than $3.2 \Omega \text{ cm}^2$ per cell pair across all tests performed with the two RED stacks we used.

2.4. Water pair testing procedure

The RED stacks were cleaned and benchmarked prior to testing each real or control water pair. After flushing the cleaning solutions from the stack, approximately 250 mL of each the concentrated and dilute feed waters were circulated in a closed loop for 15 min to allow the voltage across the membranes to stabilize (defined as achieving a rate of voltage change lower than approximately $\pm 0.2 \text{ mV s}^{-1}$).

After 15 min, we replaced the concentrated and dilute waters in the feed reservoirs and began pumping in a single-pass configuration. Waters were pumped continuously in counter-current flow configuration at 216 mL min^{-1} , corresponding to a crossflow velocity (i.e., not accounting for the volume occupied by the spacer) of approximately 1 cm s^{-1} parallel to the surface of the membranes inside the stack. Previous studies showed that counter-current flow configuration improved the energy efficiency of RED relative to co-current flow [36], and that a velocity of 1 cm s^{-1} was a reasonable tradeoff between maximizing power density (via reduced concentration polarization) and minimizing pumping losses [6,37].

The RED stack was connected to a potentiostat (VMP3, Bio-Logic Science Instruments, France), which was used to measure the electrical performance of the stack. The test method contained four serial tasks: (1) OCV measurement for 1 min, (2) linear sweep voltammetry (LSV) to obtain the stack resistance, (3) nine constant-current steps (i.e., chronopotentiometry, CP) lasting 1 min each, and (4) a 15 s OCV recovery period followed by a final LSV measurement. The current steps were adjusted for each water pair to ensure that the test protocol captured the maximum power density. During the current step corresponding to the maximum power density, we collected effluent samples from both the concentrated and dilute compartments for subsequent analysis (see [Section 2.5](#)). The sequence of electrical performance measurements (OCV, LSV, CP, LSV) was repeated three times without stack disassembly. All tests were carried out at room temperature ($\sim 20^\circ \text{C}$).

2.5. Ionic composition, dissolved organic carbon, and UV absorbance

We determined the ionic composition of both influent and effluent waters by ion chromatography. The target ions for analysis comprised Na^+ , Cl^- , Mg^{+2} , Ca^{+2} , K^+ , and SO_4^{-2} for all waters, and also included NO_3^- and NH_4^+ for the pickling brine. The ions were selected based on the expected composition of seawater [38], wastewater effluent [39], and pickling brine [40]. We also attempted to analyze for acetate in the pickling brine, but were unable to detect it due to interference from the high Cl^- content of this water. Ions except for NH_4^+ and NO_3^- were analyzed on a Dionex DX-500 ion chromatograph with conductivity detection, and CS12 and AS23 columns for detection of cations and anions, respectively. NH_4^+ and NO_3^- were analyzed with a Lachat model QC-8000 flow injection analyzer with colorimetric detectors.

We measured the dissolved organic carbon (DOC) content of water samples using a TOC-V analyzer (Shimadzu, Atlanta, GA), and UV absorbance at 254 nm (UVA_{254}) with a U-2000 spectrophotometer (Hitachi Instruments Inc., Danbury, CT) using a 1 cm quartz cell. Prior to DOC and UVA_{254} measurements, we filtered samples through $0.45 \mu\text{m}$ PTFE syringe filters (Corning Inc., Corning, NY). Specific UV absorbance (SUVA) was calculated as $100 \cdot (\text{UVA}_{254} \cdot \text{DOC}^{-1})$. It should

be noted that suspended organic carbon that may have passed through the $10 \mu\text{m}$ prefilters was not accounted for in these measurements.

2.6. Statistical analysis

We constructed 95% confidence intervals ($p = 0.05$) to determine the statistical significance of differences between two groups of data, based on common practice. Differences between two variables were deemed significant when the confidence intervals did not overlap. When performing linear correlations, we averaged the values of replicate measurements for the independent variable, and correlated these averages with individual replicate values for the dependent variable. Linear correlations were performed using R (version 3.3.1) [41].

3. Theory

Two primary metrics characterize the performance of natural water pairs in RED: power density and energy extraction efficiency. Power density is determined by the OCV, membrane permselectivity, and stack resistance. Energy extraction efficiency measures how much of the available mixing energy is converted into electricity. We introduce each of these metrics below.

3.1. Power density

The maximum power density has a significant influence on RED system feasibility because, for a desired amount of power output, the power density determines the quantity of ion exchange membranes that are required. The maximum power density (P_{max} , W m^{-2}) obtainable from a RED stack depends on the OCV (V) and the total stack resistance (R_{tot} , Ω) according to [42]

$$P_{max} = \frac{OCV^2}{8NAR_{tot}}, \quad (1)$$

where A (m^2) is the cross-sectional area of a single membrane and N (dimensionless) is the number of cell pairs in the stack. Eq. (1) is equivalent to the well-known Maximum Power Transfer theorem, where the power has been divided by the total membrane area $2NA$ to obtain units of W m^{-2} .

3.2. Energy extraction efficiency

A second performance metric for RED systems is the energy extraction efficiency (η , dimensionless), which is defined as the ratio of the energy recovered by the system as electricity ($W_{extracted}$, J m^{-3}) to the total mixing energy (W_{ideal} , J m^{-3}) available for extraction from the respective feed waters [36,43]. Energy extraction efficiency is given by

$$\eta = \frac{W_{extracted}}{W_{ideal}}, \quad (2)$$

where both $W_{extracted}$ and W_{ideal} are expressed per unit volume of blended (i.e., effluent) solution. $W_{extracted}$ can be calculated from the obtained power density as

$$W_{extracted} = \frac{2NAP_{max}}{Q}, \quad (3)$$

where Q ($\text{m}^3 \text{ s}^{-1}$) is the total flow rate through a single cell pair, and the total active membrane area $2NA$ converts P_{max} from W m^{-2} to W . The maximum energy that can be extracted from blending two salt solutions in an ideal thermodynamic process is equal to the Gibbs free energy of mixing (ΔG_{mix} , J) [35,36,43]. Hence,

$$W_{ideal} = \frac{\Delta G_{mix}}{V_B} = \frac{\Delta G_B - \Delta G_C - \Delta G_D}{V_B} \quad (4)$$

and

$$\Delta G_{B,C, \text{ or } D} = RT \sum_i n_i \ln \gamma_i C_i, \quad (5)$$

where n_i (mol) is the number of moles of species i , V_B (m^3) is the total volume of blended solution, R ($8.314 \text{ J mol}^{-1} \text{ K}^{-1}$) is the ideal gas constant, T (K) is the absolute temperature, and the subscripts B , C and D denote blended, concentrated, and dilute solutions, respectively. Since the concentrated and dilute waters are fed to the RED stack at equal rates (i.e., blending ratio of 1:1), Eqs. (4) and (5) can be conveniently solved by setting $V_B = 1L$, $n_i =$ the molar concentration in the blended effluent when calculating ΔG_B , and $n_i =$ one-half the molar concentration in the corresponding influent when calculating ΔG_C or ΔG_D (i.e., blending of 0.5 L of each solution).

3.3. Open circuit voltage and permselectivity of multicomponent salt solutions

The OCV of a RED stack arises from the combined potentials across each ion exchange membrane, which represents the potential required to oppose the diffusion of counter-ions through the membrane. For single-salt solutions, the potential of an ideally-selective membrane (OCV_i , V) is calculated using the Nernst equation [16,44,45]

$$OCV_i = \frac{RT}{zF} \ln \frac{\gamma_C C_C}{\gamma_D C_D}, \quad (6)$$

where C (mol L^{-1}) and γ (dimensionless) are the concentration and activity coefficients, respectively, of the counter-ion (i.e., the ion with opposite charge to the membrane), subscripts C and D refer to the concentrated and dilute solutions, respectively, z is the total charge of the counter-ion, and F (96485 C mol^{-1}) is the Faraday constant.

We can then calculate the ideal OCV of the entire RED stack (OCV_{ideal} , V) by multiplying OCV_i by the total number of membranes in the stack ($2N$). Hence,

$$OCV_{ideal} = 2NOCV_i. \quad (7)$$

The stack permselectivity (α , dimensionless) is defined as the ratio between the measured OCV_{meas} and OCV_{ideal} [6,45,46],

$$\alpha = \frac{OCV_{meas}}{OCV_{ideal}}, \quad (8)$$

and represents the average permselectivity of both the cation and anion exchange membranes (CEMs and AEMs).

In a single-salt solution, there is only one counter-ion to define OCV_i , and application of Eq. (6) is straightforward. However, in multicomponent solutions such as the real waters used in this work, each counter-ion species initially has a unique concentration gradient. The final membrane potential (OCV_i) is established through an ion-exchange process, in which counter-ions in one solution exchange across the membranes for counter-ions in the adjacent solution, altering their respective concentrations until each counter-ion species has an OCV equal to OCV_i [15,16]. As a result, ions with a small initial concentration gradient may be transported against their concentration gradient (i.e., from low to high concentration) by exchanging with ions that have a larger initial concentration gradient [16,19,22,24].

Vermaas et al. [16] developed an equation to solve for OCV_i when two counter-ions (e.g., Na^+ and Mg^{+2}) are present. We generalized their equation to accommodate a complex feed water containing many counter-ion species. In this case, it is necessary to solve for the change in concentration of each counter-ion species (ΔC_g , mol L^{-1}), that results in the same OCV (equal to OCV_i) for all species. When ΔC_g is considered, Eq. (6) becomes

$$\begin{aligned} OCV_i &= \frac{RT}{z_{g1}F} \ln \frac{\gamma_C(C_{C1} - \Delta C_{g1})}{\gamma_D(C_{D1} + \Delta C_{g1})} = \frac{RT}{z_{g2}F} \ln \frac{\gamma_C(C_{C2} - \Delta C_{g2})}{\gamma_D(C_{D2} + \Delta C_{g2})} \dots \\ &= \frac{RT}{z_{gi}F} \ln \frac{\gamma_C(C_{Ci} - \Delta C_{gi})}{\gamma_D(C_{Di} + \Delta C_{gi})}, \end{aligned} \quad (9)$$

where a positive ΔC_g is associated with a movement of the counter-ion from the concentrated to the dilute compartment, and the subscript gi denotes counter-ion species. The activity coefficients are assumed constant because the concentration changes are expected to be small relative to the initial concentrations ($\Delta C_g \ll C$). Assuming equal volumes of concentrated and dilute solutions, electroneutrality of the ion-exchange process requires that

$$\sum_i^n z_{gi} \Delta C_{gi} = 0, \quad (10)$$

where the summation extends over all the counter-ions (i) for a particular membrane. Solving Eq. (9) and Eq. (10) yields OCV_i across an AEM or CEM for an arbitrary mixture of ions, and can be used to determine the permselectivity according to Eq. (8).

In solving Eqs. (9) and (10) for a given water pair, we considered all ions that individually contributed $> 0.5\%$ to the total equivalent charge (Na^+ , Cl^- , Mg^{+2} , SO_4^{-2} , K^+ , and Ca^{+2} ; see Section 4.1); combined, these ions contributed more than 99.7% of the total equivalent charge. We used activity coefficients for ions in seawater from Mistry et al. [47] for the concentrated solutions, and nonlinear solver software (Excel 2013, Microsoft Corporation) to determine OCV_i . We considered this approach valid because the solved ΔC_g were consistent with the mechanism proposed by Vermaas et al. [16] in which multivalent ions transport against their concentration gradient and exchange for monovalent ions in order to establish equilibrium (see Supplementary material).

3.4. Stack resistance

The resistance of a RED stack to ionic current characterizes the amount of energy lost due to the interaction between the ions and the various components of the stack. Total stack resistance can be expressed as

$$R_{tot} = R_C + R_D + R_M + R_{SS} + R_{non-ohmic}, \quad (11)$$

where R_C and R_D represent the resistances of the concentrated and dilute feed water compartments, respectively, R_M is the ion exchange membrane resistance, R_{SS} is the resistance due to the “spacer shadow effect,” and $R_{non-ohmic}$ is the non-ohmic resistance. R_M represents the intrinsic resistance of the membranes to ion transport. R_{SS} accounts for the fact that the presence of a spacer in the solution compartment reduces the membrane area available for ionic current transport, and is directly proportional to the membrane resistance [35]. $R_{non-ohmic}$ can be attributed primarily to the resistance of the diffusion boundary layer [35]. R_C or R_D can be calculated based on the conductivity of the respective feed waters as

$$R_C \text{ or } R_D = \frac{N\delta_S}{A\epsilon^2\kappa}, \quad (12)$$

where N (dimensionless) is the number of concentrated or dilute solution compartments, δ_S (0.00045 m) is the thickness of the solution flow channels, ϵ (dimensionless) is the porosity of the spacer material and κ (S m^{-1}) is the solution conductivity. Additional details about how we determined the various components of resistance from our measurements are available in the Supplementary material. Values of R_{tot} , R_C , R_D , R_M , R_{SS} and $R_{non-ohmic}$ reported below were multiplied by $\frac{A}{N}$ to obtain units of $\Omega \text{ cm}^2 \text{ cell pair}^{-1}$.

4. Results and discussion

4.1. Water quality

The major characteristics of each source water are summarized in Table 2. The salinity gradients ranged from 3.8 (RO/GW) to 104.5 (SW/WW), where the salinity gradient is defined as the conductivity ratio between the two waters. Although the OCV of an RED stack is

Table 2
Source water characteristics. For each water pair, the concentrated feed water is shown on the left and the accompanying dilute feed water is shown on the right.

Water pair	RO/GW		SW/BW		NaCl/NaCl		PK/ST		SW/RW		SW/WW	
	RO brine	Ground water	Sea water	Brackish water	30 g L ⁻¹ NaCl	1 g L ⁻¹ NaCl	Pickling brine	Storm water	Sea water	Rain water	Sea water	WWTP effluent
Conductivity ^a , mS cm ⁻¹	31.3	8.3	46.2	3.1	43.4	1.8	103.3	3.6	46.2	1.01	46.2	0.44
Conductivity ratio ^b	3.8		14.8		23.8		28.9		45.7		104.5	
pH ^b	8.0	7.0	7.0	5.8	5.5	5.5	3.5	8.4	7.0	5.0	7.0	6.8
DOC ^c , mg L ⁻¹	19.5 ± 0.2	4.1 ± 0.1	2.8 ± 0.1	15.3 ± 0.1	n/a	n/a	8033 ± 20	20.9 ± 0.1	2.8 ± 0.1	6.4 ± 0.1	2.8 ± 0.1	16.3 ± 0.1
UVA ₂₅₄ ^c , cm ⁻¹	0.225 ± 0.002	0.055 ± 0.001	0.016 ± 0.001	0.232 ± 0.008	n/a	n/a	0.645 ± 0.002	0.193 ± 0.004	0.016 ± 0.001	0.136 ± 0.002	0.016 ± 0.001	0.167 ± 0.006
SUVA ^c , L mg ⁻¹ m ⁻¹	1.16 ± 0.01	1.34 ± 0.03	0.57 ± 0.02	1.52 ± 0.02	n/a	n/a	0.01 ± 0.00	0.92 ± 0.02	0.57 ± 0.02	2.13 ± 0.05	0.57 ± 0.02	1.02 ± 0.04

^a Field measurement based on the raw, unfiltered sample.

^b Calculated as the ratio of the conductivity in the concentrated water to that of the dilute water.

^c After filtration through 10 μm polypropylene felt and 0.45 μm PTFE filters. Reported values represent the average and standard deviation of three measurements of the same sample.

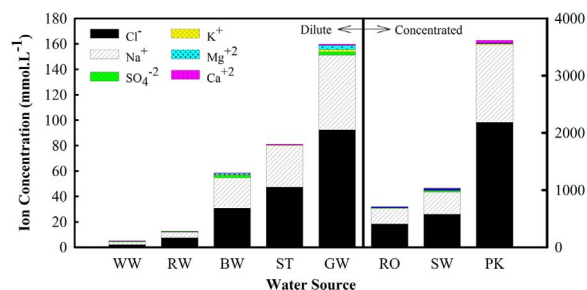


Fig. 2. Ionic composition of the real waters. Dilute feed waters are shown in the left panel and concentrated feed waters are shown in the right panel. WW = wastewater; RW = rainwater; BW = brackish surface water; ST = stormwater; GW = brackish groundwater; RO = reverse osmosis brine; SW = seawater; PK = pickling brine. Note the different scales in the y-axes for the dilute (left) and concentrated (right) waters.

determined by the activity ratio of the respective feed waters (see Eq. (6)), it is not possible to define a single activity ratio for water pairs containing more than one salt. Therefore, we report the conductivity ratio to give an approximate indication of each water pair's potential for RED power generation. In Section 4.4 we show quantitatively that the conductivity ratio provides an accurate estimate of the OCV for such water pairs.

All waters fell within a pH range of 5.0–8.4, with the exception of PK, which had a pH of 3.5. The organic carbon content of the waters varied widely, from 2.8 mg L⁻¹ in SW to more than 8 g L⁻¹ in PK. UVA₂₅₄ and SUVA ranged from 0.016 cm⁻¹ (SW) to 0.645 cm⁻¹ (PK) and from 0.01 L mg⁻¹ m⁻¹ (PK) to 2.13 L mg⁻¹ m⁻¹ (RW), respectively. The low pH and extremely low SUVA value for PK are consistent with expectations based on the composition of similar pickling brines, which are known to contain aliphatic organic acids such as lactic and acetic acid [40].

Ionic composition results (Fig. 2) show that Na⁺ and Cl⁻ accounted for the vast majority of the ions in all waters (82–99% on a molar basis). K⁺, Mg²⁺, Ca²⁺ and SO₄²⁻ were all detected in every water except for WW (which lacked K⁺ and Mg²⁺) and ST (which lacked Mg²⁺). Low amounts of NH₄⁺ (< 10 mM, not shown) were present in PK, while traces of NO₃⁻ (< 30 μM, not shown) were found in ST. Detailed ionic composition information is available in the Supplementary material.

It is unsurprising that several of the studied waters had ionic compositions dominated by Na⁺ and Cl⁻, considering that many of them derive from natural seawater. Seawater intrusion into the water table results in brackish groundwater, RO brine is a concentrated form of the brackish groundwater, and the brackish surface water is the result of dilution of seawater with river water. In contrast, the wastewater effluent, pickling brine, rainwater, and stormwater are not influenced by the sea, which is reflected in their ionic composition. For example, the Ca²⁺ content of these waters was higher than that of the seawater-influenced waters, and the Mg²⁺ content was lower.

Towards deciding which ions were important to consider for the calculation of OCV_i (Eqs. (9) and (10)) and other relevant system properties, we evaluated the relative importance of individual ions to the overall ionic composition based on equivalent charge (z_iC_i). The only ions that contributed individually more than 0.5% of the total equivalent charge to any water were Na⁺, Cl⁻, Mg²⁺, SO₄²⁻, K⁺, and Ca²⁺, and combined they always contributed more than 99.7% of the total equivalent charge. Therefore, we focused all relevant analyses below on these ions.

4.2. Power density

The maximum power density obtained from each of the water pairs is shown in Fig. 3 (red bars) and in Table S5. Maximum power densities ranged from 0.07 W m⁻² for the RO/GW water pair to 0.59 W m⁻² for the PK/ST water pair. The water pairs with the highest power densities (PK/ST and NaCl/NaCl) were those with intermediate conductivity

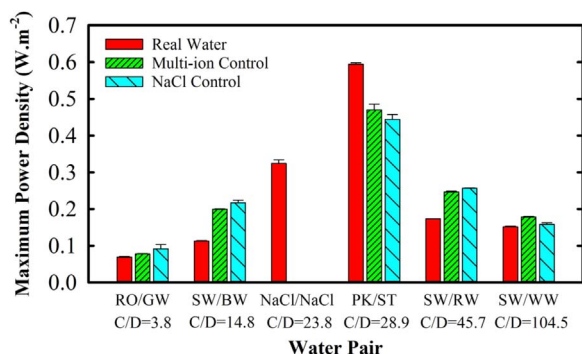


Fig. 3. Maximum power densities obtained from real water pairs (red bars), multi-ion controls (green hatched bars), and NaCl controls (blue bars). For each water pair, RED tests for the real waters, multi-ion control, and NaCl control were performed at the optimum current density for the real waters. Error bars represent the standard deviation between at least three replicates. The C/D ratios below the x-axis labels indicate the conductivity ratio (concentrated/dilute) for the water pair. (For interpretation of the references to color in this figure legend, the reader is referred to the web version of this article).

ratios (28.9 and 23.8, respectively). On the other hand, the water pairs with the highest conductivity ratios (SW/WW, 104.5 and SW/RW, 45.7) had mediocre power densities. These power density results demonstrate an inherent tradeoff in RED. Very large concentration gradients are beneficial for power output because they increase the OCV (see Eq. (6)), but achieving such gradients generally entails using very low concentrations for the dilute feed water. The low conductivity of the dilute feed water limits power output by increasing the stack resistance, which we discuss further in Section 4.6. Thus, the power output is sensitive to both the ratio between the respective salt concentrations, and the magnitude of the dilute salt concentration.”

In addition to considering the salinity gradient of each water pair, it is also useful to compare the performance of the real water pairs with that of synthetic “seawater” and “river water” (i.e., the NaCl/NaCl water pair). The PK/ST water pair was the only real water pair with a higher power density than the NaCl/NaCl water pair; maximum power densities for the other real water pairs were all less than 55% of that obtained from the NaCl/NaCl water pair. Overall, the power densities in this work (0.07–0.59 W m⁻²) were comparable to those obtained in other studies of natural waters (0.1–1.6 W m⁻²) [5,7,22,26,48] and lower than those obtained in studies of synthetic waters (1–4 W m⁻²) [1,4,5,7,26]. In particular, the power density of the NaCl/NaCl water pair (0.32 W m⁻²) was very similar to the power density obtained by Zhu et al. (0.28 W m⁻²) using a nearly-identical PCCell stack and similar concentrations of NaCl [17]. Other studies have obtained higher power densities (0.65–1.28 W m⁻²) using the same concentration gradient, but these studies employed stacks with thinner spacers (~200 μm vs. 450 μm in this work), which would have reduced the stack resistance and enabled higher performance [1]. Thus, the power densities we observed are consistent with other reports in the literature. The relatively poor performance of most real water pairs compared to the commonly-studied synthetic “seawater” and “river water” pair illustrates the potentially severe detrimental impacts that NOM and inorganic solutes can have on RED performance.

We will now consider the impact of NOM on the obtained power density by comparing the performance of the real water pairs (Fig. 3, red bars) with the multi-ion controls (Fig. 3, green hatched bars). The power densities obtained from multi-ion controls were 13–77% higher than those obtained from the corresponding real water pair, with the exception of the PK/ST water pair. For the PK/ST water pair, the power density of the multi-ion control was 21% lower than that of the real water. All differences in power densities were statistically significant.

Since the only difference between the real water pairs and the multi-ion controls was the presence of NOM, these findings indicate that NOM had a large negative impact on the RED performance of most real water

pairs. Vermaas et al. observed detrimental impacts of natural foulants, including NOM, clay, and microorganisms, on RED performance (i.e., increasing stack resistance and decreasing OCV) over a period of about 24 h [22], but we are unaware of any studies that have measured the “instantaneous” impact of NOM in a short-duration experiment. Although negative impacts of NOM on power density appear to be common, the fact that the presence of NOM in the PK/ST water pair increased power density suggests that specific characteristics of the NOM can alter its impact on performance. This finding is in agreement with several studies from the ED literature, which showed that fouling behavior is largely determined by the specific properties of the organic matter (e.g., size, hydrophobicity, aromaticity, or charge) rather than its concentration [29–31,49]. As noted in Section 4.1, the extremely high DOC concentration (~8 g L⁻¹) and low SUVA (0.01 L mg⁻¹ m⁻¹) of the PK water set it apart from the other waters tested (2.8–20.9 mg L⁻¹ DOC and 0.57–2.13 L mg⁻¹ m⁻¹ SUVA). We will discuss the possible influence of these unique NOM characteristics further in Section 4.6.

In addition to the impacts of NOM, we evaluated the effect of inorganic solutes on RED performance by comparing the multi-ion controls (Fig. 3, green hatched bars) with the corresponding NaCl controls (Fig. 3, blue bars). Statistically significant differences between multi-ion and NaCl controls occurred only for water pairs involving SW (i.e., SW/RW, SW/WW, and SW/BW) and were always smaller than 13%. Specifically, inorganic solutes lowered the power density for the SW/RW and SW/BW water pairs by 4% and 8%, respectively, while increasing power density for the SW/WW water pair by 13%. Several other studies [19,23,24] have shown that the presence of multivalent ions such as Mg⁺² can lower OCV and increase stack resistance, leading to reduced power density. However, we are unaware of any reports of ions increasing power density in the peer-reviewed literature. This unexpected result for the SW/WW water pair is a consequence of the higher OCV of the multi-ion control compared to the NaCl control, which we consider an anomaly (see Section 4.4). Overall, the impact of inorganic solutes on the obtained power density was considerably smaller than the impact of NOM. This finding underscores the importance of understanding interactions between NOM and ion exchange membranes to evaluate practical applications of RED.

Finally, we compare the performance of the real water pairs (Fig. 3, red bars) with that of the NaCl controls (Fig. 3, blue bars) in order to quantify the combined effects of ions and NOM on performance. In general, the power densities obtained from real water pairs were lower than those obtained from the corresponding NaCl control water pairs, suggesting that the constituents in the real water pairs studied had a negative impact on performance. Specifically, the power densities of the RO/GW, SW/BW, SW/RW, and SW/WW water pairs were 4–48% lower than those of the corresponding NaCl controls. The PK/ST water pair was the only pair for which the real water pair outperformed the NaCl control, and we hypothesize that this unexpected result is a consequence of unique interactions between the NOM and pH gradients in this particular water pair (see Section 4.6).

4.3. Energy extraction efficiency

Our RED stacks extracted 0.34–1.61 W h per m³ of mixed solution with corresponding efficiencies in the range of 0.37% (SW/BW) to 1.05% (NaCl/NaCl) (see values in Supplementary material). Such low efficiencies are not surprising for single pass experiments with small RED stacks having short residence times (i.e., 8 s in our case). For example, using a similar concentration gradient, stack geometry, and residence time, Vermaas et al. achieved energy efficiencies of 1–2% [50], and Tedesco et al. [6] reported efficiencies of approximately 1% when testing highly concentrated NaCl brines. Higher efficiencies (50–77%) were reported in other studies [4,11] using pure NaCl solutions in closed-loop systems over a wide range of concentrations and conductivity ratios. Recent modeling efforts have suggested that higher

efficiencies in the range of 10–20% could be achieved in scaled-up systems with longer residence times and other optimized conditions [51].

Energy extraction efficiencies from the multi-ion controls ranged from 0.34% to 0.82%, and were 0.07–0.28% points higher than those of the corresponding real water pairs (0.37–0.69%), except for the PK/ST water pair for which the efficiency of the multi-ion control (0.34%) was 0.09% points lower. All differences were statistically significant. As was the case with power density, this finding indicates that the presence of NOM has an adverse effect on energy extraction by RED, but that specific NOM characteristics can reverse the effect (e.g., in the case of the PK/ST water).

To further investigate the impacts of NOM characteristics on energy extraction efficiency, we examined the statistical correlation between the energy extraction efficiency and the DOC or UVA_{254} content of the concentrated and dilute waters (Fig. S1). We found a strong correlation between efficiency and the UVA_{254} of the dilute waters ($R^2 = 0.90$, $p < 0.001$), and a moderately strong correlation with the DOC of the dilute waters ($R^2 = 0.82$, $p < 0.001$). No correlations were found between efficiency and the DOC or UVA_{254} of the concentrated waters. Taken together, this set of correlations indicates that the presence of UV-absorbing organic matter in the dilute feed water has a strong negative impact on RED performance. We hypothesize that osmosis from the dilute compartment to the concentrated compartment led to accumulation of organics that enhanced concentration polarization near the membrane surface, reducing the effective concentration gradient. In addition to lowering the energy efficiency, this lower gradient would result in a lower OCV, which we also observed (see Section 4.4). This explanation is consistent with the observations of Pawlowski et al. [27], who observed transport of humic acids from the dilute to the concentrated compartment of a RED stack. The fact that the performance impacts we observed were correlated with UVA_{254} is consistent with reports from the ED literature that aromatic [52] or hydrophobic [29] organic molecules tend to foul ion exchange membranes in ED stacks to a greater degree than aliphatic or hydrophilic organic molecules. Differences in the colloidal stability of NOM in high and low ionic strength waters may also influence conditions near the membrane surface. For example, low ionic strength has been shown to increase the adsorption of NOM on AEMs [31,32]. Thus, the combination of low ionic strength and high UVA_{254} in our real water dilute chambers likely promoted accumulation of NOM near the membrane surface.

The impact of inorganic solutes on energy efficiency, as determined by comparing the energy efficiency of the multi-ion controls to that of the NaCl controls, was less significant than the impact of NOM. The energy efficiencies of the NaCl controls (0.32–0.91%) were 0.03–0.14% points higher than those of the multi-ion controls (0.34–0.82%) for the SW/BW, SW/RW, and RO/GW water pairs, and 0.02–0.05% points lower than those of the multi-ion controls for the SW/WW and PK/ST water pairs. Differences were only statistically significant for the water pairs containing seawater (SW/BW, SW/RW, SW/WW).

In general, the combined effects of NOM and inorganic solutes had a significant detrimental effect on energy extraction efficiency. As noted above, energy efficiency of the real waters ranged from 0.37% to 0.69% (excluding the NaCl/NaCl pair), while that of the NaCl controls ranged from 0.32% to 0.91%. In every case except for the PK/ST water pair, the efficiency of the NaCl control was higher than that of the real water. This finding further underscores our conclusions from the power density results that the constituents of real water pairs reduce RED performance.

4.4. Open circuit voltage

Towards building a better understanding of the factors why NOM and inorganic species impacted performance, we will now consider the OCV of each water pair, which impacts both the power density (Eq. (1)) and the energy extraction efficiency (Eqs. (2) and (3)). The OCV of the

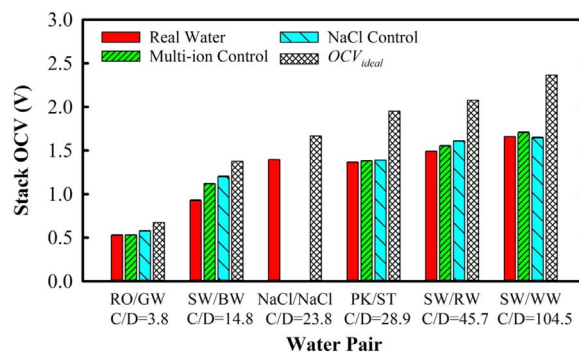


Fig. 4. Comparison of OCV of real waters (red bars), multi-ion controls (green hatched bars), and NaCl controls (blue bars) measured in a RED stack to OCV_{ideal} calculated using Eqs. (7), (9), and (10) (diagonal crosshatched bars) for six water pairs. For each water pair, the standard deviation between at least three replicate tests performed in series was less than 12 mV. C/D ratios below each x-axis label indicate the conductivity ratio between the respective concentrated and dilute feed waters. (For interpretation of the references to color in this figure legend, the reader is referred to the web version of this article).

real water pairs varied from 0.53 to 1.66 V (Fig. 4, red bars), and the sequence of OCV values generally followed the sequence of concentration ratios, as expected from the Nernst equation (Eq. (6)).

Comparing the measured OCV of the real water pairs (red bars) with those of the multi-ion control water pairs (Fig. 4, green hatched bars), illustrates the impact of NOM on the OCV. The OCV of the multi-ion controls were 0.2–4% higher than the OCV of the corresponding real water pairs for all water pairs except SW/BW, for which the OCV of the multi-ion control was 21% higher. The differences were statistically significant for all water pairs except for the RO/GW water pair. These findings indicate that the presence of NOM in the real waters negatively impacted OCV. It is striking that in the two water pairs with the highest DOC concentrations (i.e., RO/GW and PK/ST), the presence of NOM had very little impact on OCV (0–1% difference between multi-ion control and real water). In both of these water pairs, the DOC concentration in the concentrated feed water was higher than that in the dilute feed water (Table 2). The reverse was true for the remaining water pairs, which all showed a larger difference between the OCV of the multi-ion control and the real water. Taken together, these findings suggest that the presence of NOM in the dilute feed water has a larger impact on the OCV than the presence of NOM in the concentrated feed water. Moreover, the lower OCV of the multi-ion controls is consistent with our hypothesis from Section 4.3 that the presence of NOM in the dilute compartment lowers the effective salt concentration gradient by increasing concentration polarization near the membrane surface.

The impact of inorganic solutes (e.g., multivalent ions) on OCV is indicated by the difference between the multi-ion controls (Fig. 4, green hatched bars) and the NaCl controls (Fig. 4, blue bars). For all water pairs, the OCV of the multi-ion control was within 8% of the OCV of the NaCl control, and all showed statistically significant differences. In general, the OCVs of the multi-ion controls were lower than those of the NaCl controls, but for the SW/WW pair, the multi-ion control had a slightly higher OCV. We attribute this anomaly to experimental error, considering that the stack resistance of the SW/WW NaCl control was also unexpectedly high (see Section 4.6).

The overall lower OCV of real water pairs compared to the multi-ion control water pairs, and of the latter compared to NaCl water pairs, is consistent with our conclusions from the power density results that the constituents of real water pairs negatively impact RED performance. It is also noteworthy that even the NaCl controls had a significantly lower OCV than the corresponding OCV_{ideal} (Fig. 4, crosshatched bars), indicating that the permselectivity of the membranes in the RED stacks was not close to ideal (i.e., not 1), as demonstrated in the next section.

Finally, since ionic composition measurements are time-consuming and costly, we evaluated an alternative method for estimating OCV_{ideal}

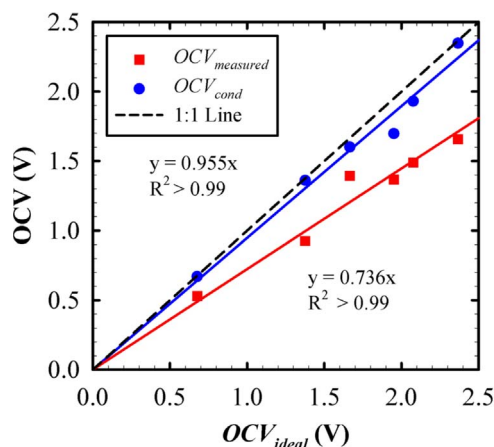


Fig. 5. Parity plot comparing OCV_{ideal} calculated from ion composition measurements (x-axis) with the measured OCV and OCV_{cond} calculated from Eq. (13) (y-axis). For the measured OCV, the slope of the regression line (forced through 0) is equal to the average apparent permselectivity of all the water pairs. For OCV_{cond} , the slope of the regression line forced through zero is very close to 1, indicating strong agreement with the calculated OCV_{ideal} .

by replacing the activity ratio in Eq. (6) with the influent conductivity ratio of the feed waters. We calculated this estimate of OCV_{ideal} for the RED stack (OCV_{cond} , V) by combining the modified Eq. (6) with Eq. (7) to obtain

$$OCV_{cond} = 2N \frac{RT}{zF} \ln \frac{\kappa_C}{\kappa_D} \quad (13)$$

While not rooted in thermodynamic principles, this “conductivity rule” is far easier to apply to complex water mixtures than the multi-ion equilibrium analysis outlined in Section 3.3. A parity plot between OCV_{cond} and OCV_{ideal} (Fig. 5, blue circles) shows that OCV_{cond} was a very good predictor of OCV_{ideal} ($R^2 > 0.99$, slope = 0.955), with OCV_{cond} being within 13% of OCV_{ideal} in all cases. Agreement was lowest for SW/WW and PK/ST (at 7% and 13% difference, respectively), while agreement was within 4% for the remaining water pairs. We attribute the larger error for SW/WW to our use of the influent conductivity ratio in Eq. (13), which may have overestimated the true average concentration ratio inside the stack. Since the WW was the most dilute water we tested, we expected salt diffusion from the concentrated compartment to substantially increase the salt concentration of the WW inside the stack. For the other water pairs, the dilute feed water was at least $2.5\times$ more concentrated than the WW, making this possible source of error less significant. For the PK/ST water pair, the conductivity ratio underestimated the concentration ratio, since the molar conductivity of NaCl decreases with concentration [53] and PK was the water with the highest salt concentration (~ 2 M NaCl). Overall, our results suggest that the “conductivity rule”, as expressed by Eq. (13), is a practical tool for evaluating water sources with complex composition for RED applications, particularly those involving moderate salinity gradients and concentrations.

4.5. Membrane permselectivity

We determined the average membrane permselectivity for each water pair as the ratio of the measured OCV to OCV_{ideal} calculated using Eqs. (9) and (10). As such, permselectivity can be visualized in Fig. 5 by comparing measured data points (red squares) with the 1:1 line. The strong linear correlation ($R^2 > 0.99$, $p < 0.001$) between OCV_{meas} and OCV_{ideal} in Fig. 5 shows that the permselectivity varied over a relatively narrow range among all the water pairs (67% for SW/BW to 84% for NaCl/NaCl; see Table S4); the slope of the regression line (73.6%) can be interpreted as the average permselectivity of the stack for all water pairs. In Fig. 5, the higher-than-average permselectivity of the NaCl/

NaCl water pair is evident from the data point at $OCV_{ideal} = 1.67$ V, which is noticeably further from the regression line than the other points. Although higher than average, the permselectivity of the NaCl/NaCl pair (84%) was lower than expected based on the nominal permselectivity of the PC-SK and PC-SA membranes used in this work (95%). However, our observed permselectivity was similar to the average permselectivity of these two membranes measured in pure NaCl (88%) by Geise et al. [18].

We attribute the lower permselectivity of the natural water pairs compared to that of the NaCl/NaCl water pair to the combined effects of concentration and specific ions. The permselectivity of ion exchange membranes depends on the concentration gradient across the membrane [4], the salt concentration on either side of the membrane [4], and on the properties of both the co-ion and counter-ion (e.g., polarizability, binding affinity, size) [18,23,24,54]. Since none of these effects is accounted for in Eq. (9), it is unsurprising that most water pairs had permselectivities lower than the NaCl control even after accounting for ion exchange between the waters. Other studies have also observed a significant reduction in OCV (and corresponding reductions in permselectivity) when RED stacks are fed with real waters compared to corresponding NaCl controls [5,7,26].

In the previous section, we observed that the presence of NOM had a significant impact on the OCV. We further explored this finding by examining linear correlations between the measured permselectivity and the DOC and UVA₂₅₄ of both the concentrated and dilute feed waters (Fig. 6). As was the case with energy extraction efficiency (see Fig. S1), we found a very strong correlation between permselectivity and the UVA₂₅₄ of the dilute water ($R^2 = 0.97$, $p < 0.001$), and a similar, but weaker correlation with the DOC of the dilute water ($R^2 = 0.78$, $p < 0.001$). No correlations were found with the DOC or UVA₂₅₄ of the concentrated feed water. These correlations further support our conclusion that the presence of UV-absorbing organic carbon in the dilute compartment of a RED stack has a significantly detrimental impact on its performance.

4.6. Stack resistance

4.6.1. Contributions of feed waters, membranes, spacers, and non-ohmic phenomena to total stack resistance of real water pairs

Together with the OCV, the stack resistance determines the overall power output of the RED stack (Eq. (1)). The total stack resistance (Fig. 7a) of real water pairs was in the 46.7–214.0 $\Omega \text{ cm}^2$ per cell pair range, and the total stack resistance of the NaCl/NaCl water pair was 69.9 $\Omega \text{ cm}^2$ per cell pair. The resistance of the NaCl/NaCl water pair was at the low end of the range obtained for real water pairs, and similar to that reported by Vermaas et al. [50] ($\sim 50 \Omega \text{ cm}^2$ per cell pair) using similar salt concentrations. As indicated by Eq. (11), the total stack resistance is the summation of the resistance contributions by the dilute (R_D) and concentrated (R_C) feed water compartments, membrane (R_M), spacer (R_{SS}), and non-ohmic phenomena ($R_{non-ohmic}$). Thus, we evaluated the relative contributions of these various components to total stack resistance.

For each of the real water pairs, the resistance of the dilute feed water compartment accounted for 21–75% of the total stack resistance, while the resistance of the concentrated feed water compartment accounted for only 1–6% (Fig. S4). Based on Eqs. (11) and (12), we examined correlations between the total stack resistance and the inverse conductivities of feed waters. We found a strong linear correlation ($R^2 = 0.90$, $p < 0.001$) between total stack resistance and the inverse conductivity of the dilute feed water, but we did not find a correlation ($R^2 < 0.01$, $p = 0.82$) between total stack resistance and the inverse conductivity of the concentrated feed water. The strong correlation with the inverse conductivity of the dilute feed water suggests that despite wide variations in inorganic and organic water quality among feed waters, the dilute feed water conductivity alone may be used as a predictor of differences in stack resistance among water pairs.

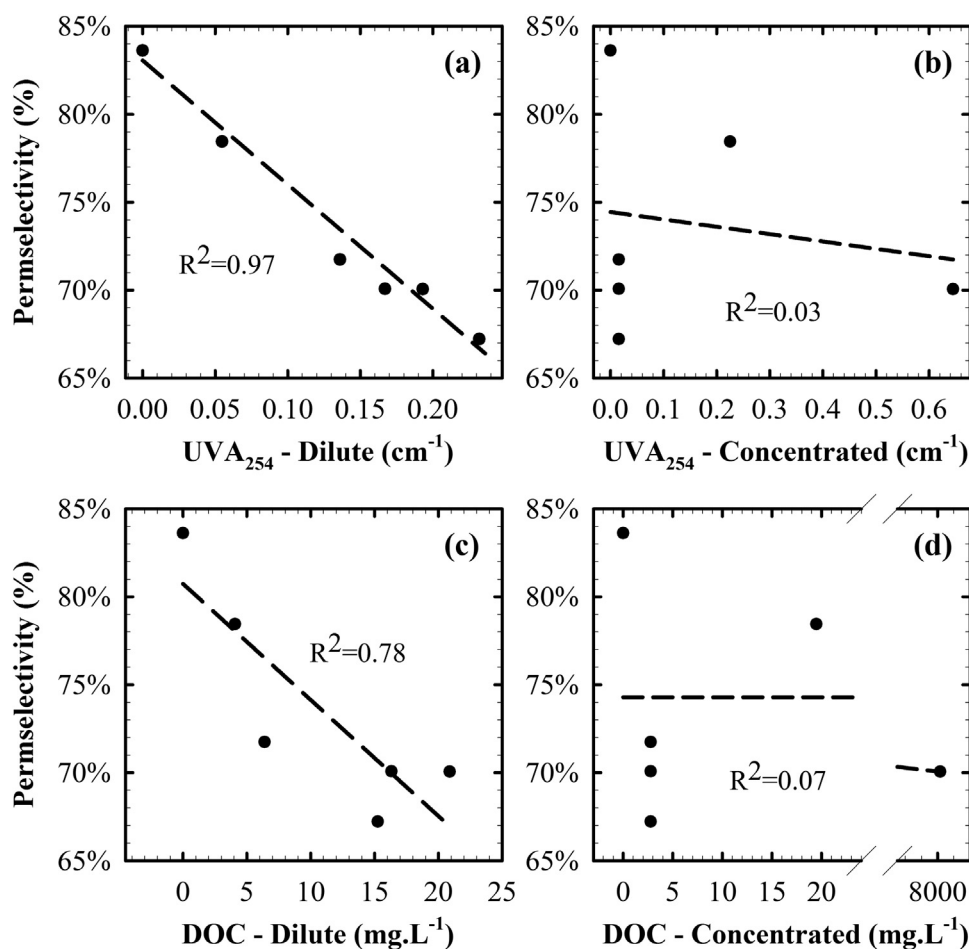


Fig. 6. Linear correlations between permselectivity and the organic carbon content, as measured by (a) UVA₂₅₄ in the dilute feed water, (b) UVA₂₅₄ in the concentrated feed water, (c) DOC concentration in the dilute feed water, and (d) DOC concentration in the concentrated feed water.

The spacer shadow effect (R_{SS}) accounted for 8–26% of total stack resistance among the real water pairs. R_{SS} is calculated based on the spacer shadow factor as a fraction of the membrane resistance (see [Supplementary material](#)). Therefore, the variation in R_{SS} among water pairs mirrors the variation in R_M , which we discuss below.

Both the membrane resistance (R_M , Fig. 7b) and non-ohmic resistance ($R_{non-ohmic}$, Fig. 7c) varied considerably among real water pairs, accounting for 11–38% and 1–9% of total stack resistance, respectively. Such variation is expected, considering that previous studies have shown that multivalent ions increase membrane resistance [5,19,21,22,24], while the presence of NOM in feed waters can induce non-uniform concentration changes (i.e., preferential channeling) within the stack that increase the non-ohmic resistance [21]. However, unlike the resistance of the solution compartments, membrane and non-ohmic resistances cannot be predicted based on water quality using existing models. As such, developing a more robust understanding of how NOM and inorganic solutes impact membrane and non-ohmic resistance in RED stacks is critically important for predicting performance with different water sources.

4.6.2. Impact of NOM on resistance

Towards developing such an understanding, we first consider the influence of NOM by comparing the resistance of the real waters (Fig. 7, red bars) with that of their multi-ion controls (Fig. 7, green hatched bars). The total stack resistance, membrane resistance and non-ohmic resistance of all real water pairs were statistically different from those of the corresponding multi-ion controls with only one exception (the non-ohmic resistances of the real RO/GW water pair and corresponding multi-ion control were not statistically different from each other). Among water pairs with significant differences, except for the PK/ST

water pair, the total, non-ohmic, and membrane resistances of the real water were 11–57%, 29–39%, and 24–235% higher, respectively, than those of the corresponding multi-ion controls. The PK/ST water pair displayed opposite trends from the others. For the PK/ST water pair, the total, non-ohmic, and membrane resistances of the real water were 16% lower, 11% lower, and 37% lower, respectively, than those of the multi-ion control. As these results illustrate, the impact of NOM on membrane resistance was considerably larger than the impact on non-ohmic resistance or total stack resistance.

To further explore the impact of NOM on membrane resistance, we related our observations to the DOC content of the feed waters in each pair. It is striking that the three real water pairs for which NOM caused the biggest increase in membrane resistance (the SW/BW, SW/RW, and SW/WW pairs) had only moderate DOC concentrations (2.8–16.3 mg L⁻¹; Table 2). However, in all three of these water pairs, the DOC concentration in the dilute feed water was higher than that in the concentrated feed water. By contrast, the membrane resistance of the PK/ST water pair was significantly lower in the real water than in the multi-ion controls, despite the presence of ~ 8 g L⁻¹ DOC in the concentrated feed water. Since moderate amounts of DOC in the dilute compartment of three water pairs increased membrane resistance, while the presence of a very large amount of DOC in the concentrated compartment of the PK/ST water pair decreased membrane resistance, our results suggest that the presence of NOM in the dilute compartment has a significant negative impact on membrane resistance in RED. This finding is consistent with studies of ED systems, which reported that NOM tends to accumulate on the surface of AEMs facing the dilute feed solution [29,32] and that NOM accumulates on AEMs to a greater degree at low ionic strength [31,32].

Furthermore, since we observed similar results for non-ohmic

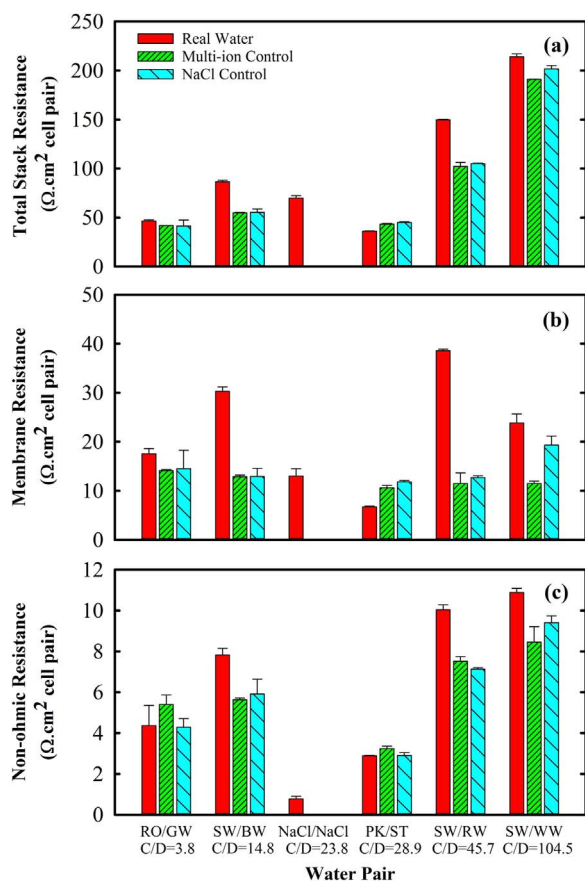


Fig. 7. (a) Total, (b) membrane, and (c) non-ohmic stack resistance of real and control water pairs. Error bars represent the standard deviation of three replicates. C/D ratios below each x-axis label indicate the conductivity ratio between the respective concentrated and dilute feed waters. (For interpretation of color in this figure legend, the reader is referred to the web version of this article).

resistance (i.e., evidence that it is negatively impacted by the presence of NOM in the dilute compartment), and that non-ohmic resistance is generally associated with boundary layer effects, we suggest that the presence of DOC in the dilute compartment hinders mass transport near the membrane surface, consistent with our observations of the impact of NOM on energy efficiency and OCV (see Sections 4.3 and 4.4, respectively). Lee et al. proposed a similar mechanism to explain increased resistance in ED stacks fouled by NOM. They suggested that electrostatic interactions between negatively-charged NOM and the positively-charged AEM cause NOM to accumulate near the membrane surface, leading to increased resistance [29].

It remains unclear why the presence of NOM appeared to lower the membrane resistance of the PK/ST pair compared to the multi-ion control, but the presence of organic acids in the PK water offers one possible explanation. The PK water was unique from the other concentrated waters in that small organic acids (e.g., acetic or lactic acids) comprised much of its NOM [40]; the very low SUVA and low pH of this water ($0.01 \text{ L mg}^{-1} \text{ m}^{-1}$, pH 3.5) were consistent with this expectation. At pH 3.5, these acids would be protonated and therefore uncharged (the pK_a for lactic and acetic acids is 3.86 and 4.76, respectively [53]), and as such would not contribute to the conductivity of the water. However, if these acids diffused through the membranes and entered the moderately alkaline ST water, they would deprotonate and increase the conductivity near the membrane surface. It is known that small neutral organic molecules can easily cross ion exchange membranes [14,30,49], and others have shown that the resistance of ion exchange membranes in the presence of a concentration difference is controlled by the conductivity of the solution at the dilute interface

[55]. As such, the appearance of dissociated acids near the surface of the membrane could have lowered its resistance.

4.6.3. Impact of inorganic species on resistance

To determine the impact of inorganic solutes on stack resistance, we now compare the resistance of the multi-ion controls (Fig. 7, green hatched bars) with that of the corresponding NaCl controls (Fig. 7, blue bars). The differences between any two corresponding resistances (total, membrane, or non-ohmic) of these two controls were insignificant for most water pairs. The only statistically significant differences observed were for the total and membrane resistances of the SW/WW water pair, which were higher in the NaCl control than in the multi-ion control. In light of the unexpectedly low OCV of this NaCl control compared to the multi-ion control (see Section 4.4), we do not consider this difference meaningful. Overall, our findings indicate that at the concentrations typically encountered in real natural waters, the presence of inorganic solutes has a negligible impact on RED stack resistance. While previous studies of synthetic waters have clearly shown that the presence of multivalent ions like Mg^{+2} increases membrane resistance compared to NaCl [5,16,19], these studies employed higher concentrations of multivalent ions than we detected in our waters. Fontananova et al. [23] tested mixtures of 0.47 M NaCl containing 0.028 M Mg^{+2} (similar to concentrations in our SW), and observed only a $0.1 \Omega \text{ cm}^2$ (7%) increase in membrane resistance compared to 0.5 M NaCl. Considering this observation, we attribute the lack of significant increases in membrane resistance to the low concentration of multivalent ions in our water pairs.

The combined impacts of NOM and inorganic solutes on resistance can be examined by comparing the resistance of the real waters (Fig. 7, red bars) to that of the NaCl controls (Fig. 7, blue bars). Excluding the PK/ST water pair, the total stack resistance of the real waters was 6–56% higher than that of the NaCl controls. As discussed in the previous paragraphs, the increased resistance of the real waters can be attributed primarily to the impact of NOM on membrane resistance. The PK/ST water pair was unique in that the real water had a lower total and membrane resistance than the NaCl control, and we attribute this result to interactions between particular NOM constituents and the pH gradient in this water pair, as described above.

5. Conclusions

In this work, we measured power generation from five real water pairs containing complex mixtures of ions and natural organic matter in laboratory-scale RED stacks. The water pairs were evaluated for power density, energy efficiency, open circuit voltage, permselectivity, and stack resistance. We compared these performance metrics and stack properties both among the real water pairs and between the real water pairs and corresponding controls, where the controls were designed to isolate the impacts of NOM and inorganic solutes on RED stack performance. We also related the RED performance metrics to common measures of water quality. The following points summarize our major findings:

- The presence of NOM impacted power density to a greater degree than the presence of inorganic solutes. NOM generally decreased the power density by up to 43%, whereas the presence of inorganic solutes decreased the power density up to 8% in most water pairs.
- The location of NOM (i.e., in the concentrated vs. the dilute feed water) altered its impact on RED performance. The presence of NOM in the dilute feed waters was associated with increased membrane resistance and lower OCVs; this was not the case for NOM presence in the concentrated feed waters. We explained these results by suggesting that the presence of NOM in the dilute compartment hinders mass transport near the membrane surface.
- UV-absorbing NOM present in the dilute waters was strongly associated with reduced membrane permselectivity and reduced energy

extraction efficiency. Neither permselectivity nor efficiency was correlated with the presence of NOM in the concentrated feed water.

- We demonstrated that the membrane potential between two waters with arbitrary ionic composition can be estimated within approximately 10% by substituting the conductivity ratio (concentrated:dilute) for the activity ratio in the Nernst equation.
- The pickling brine/stormwater pair behaved differently from the others in that the presence of NOM in the pickling brine increased its performance relative to controls (e.g., power densities of 0.59 and 0.44 W m⁻² for the real water pair and NaCl / NaCl control, respectively). We attribute this unique behavior to the presence of a large pH gradient (~ 5 units) between the two waters and the characteristics of the DOC in the pickling brine (such as the presence of small organic acids).
- The high performance of the pickling brine/stormwater pair suggests that RED may have promise for industrial energy recovery applications.

Acknowledgements

This work was funded by the University of North Carolina Research Opportunities Initiative (ROI) program. R. Kingsbury was supported by the Duke Energy Fellowship and the National Science Foundation Graduate Research Fellowship Program under Grant no. DGE-1144081. Any opinions, findings, and conclusions or recommendations expressed in this material are those of the authors and do not necessarily reflect the views of the National Science Foundation. We also wish to thank the staff at Jennette's Pier, Pine Island Nature Preserve, Mt. Olive Pickle Company, and the Kill Devil Hills Water Treatment Plant for their assistance and support in acquiring water samples. We also acknowledge the staff of the North Carolina State University Soils Laboratory for their assistance with ion chromatography analyses.

Appendix A. Supporting information

Supplementary data associated with this article can be found in the online version at <http://dx.doi.org/10.1016/j.memsci.2017.07.038>.

References

- [1] J. Gi, B. Zhang, S. Glabman, N. Uzal, X. Dou, H. Zhang, X. Wei, Y. Chen, Potential ion exchange membranes and system performance in reverse electro dialysis for power generation: a review, *J. Membr. Sci.* 486 (2015) 71–88.
- [2] O.A. Alvarez-Silva, A.F. Osorio, C. Winter, Practical global salinity gradient energy potential, *Renew. Sustain. Energy Rev.* 60 (2016) 1387–1395, <http://dx.doi.org/10.1016/j.rser.2016.03.021>.
- [3] A. Daniilidis, R. Herber, D.A. Vermaas, Upscale potential and financial feasibility of a reverse electro dialysis power plant, *Appl. Energy* 119 (2014) 257–265, <http://dx.doi.org/10.1016/j.apenergy.2013.12.066>.
- [4] A. Daniilidis, D.A. Vermaas, R. Herber, K. Nijmeijer, Experimentally obtainable energy from mixing river water, seawater or brines with reverse electro dialysis, *Renew. Energy* 64 (2014) 123–131, <http://dx.doi.org/10.1016/j.renene.2013.11.001>.
- [5] R.A. Tufa, E. Curcio, W. van Baak, J. Veerman, S. Grasman, E. Fontananova, G. Di Profio, Potential of brackish water and brine for energy generation by salinity gradient power-reverse electro dialysis (SGP-RE), *RSC Adv.* 4 (2014) 42617–42623, <http://dx.doi.org/10.1039/C4RA05968A>.
- [6] M. Tedesco, E. Brauns, A. Cipollina, G. Micale, P. Modica, G. Russo, J. Helsen, Reverse Electro dialysis with saline waters and concentrated brines: a laboratory investigation towards technology scale-up, *J. Membr. Sci.* 492 (2015) 9–20, <http://dx.doi.org/10.1016/j.memsci.2015.05.020>.
- [7] M. Tedesco, C. Scalici, D. Vaccari, A. Cipollina, A. Tamburini, G. Micale, Performance of the first reverse electro dialysis pilot plant for power production from saline waters and concentrated brines, *J. Membr. Sci.* (2015), <http://dx.doi.org/10.1016/j.memsci.2015.10.057>.
- [8] M. Tedesco, A. Cipollina, A. Tamburini, G. Micale, J. Helsen, M. Papapetrou, REAPower: use of desalination brine for power production through reverse electro dialysis, *Desalin. Water Treat.* 53 (2014) 3161–3169, <http://dx.doi.org/10.1080/19443994.2014.934102>.
- [9] X. Luo, X. Cao, Y. Mo, K. Xiao, X. Zhang, P. Liang, X. Huang, Power generation by coupling reverse electro dialysis and ammonium bicarbonate: implication for recovery of waste heat, *Electrochem. Commun.* 19 (2012) 25–28, <http://dx.doi.org/10.1016/j.elecom.2012.03.004>.
- [10] K. Kwon, B.H. Park, D.H. Kim, D. Kim, Parametric study of reverse electro dialysis using ammonium bicarbonate solution for low-grade waste heat recovery, *Energy Convers. Manag.* 103 (2015) 104–110, <http://dx.doi.org/10.1016/j.enconman.2015.06.051>.
- [11] R.S. Kingsbury, K. Chu, O. Coronell, Energy storage by reversible electro dialysis: the concentration battery, *J. Membr. Sci.* 495 (2015) 502–516, <http://dx.doi.org/10.1016/j.memsci.2015.06.050>.
- [12] W.J. van Egmond, M. Saakes, S. Porada, T. Meuwissen, C.J.N. Buisman, H.V.M. Hamelers, The concentration gradient flow battery as electricity storage system: technology potential and energy dissipation, *J. Power Sources* 325 (2016) 129–139, <http://dx.doi.org/10.1016/j.jpowsour.2016.05.130>.
- [13] W.J. van Egmond, U.K. Starke, M. Saakes, C.J.N. Buisman, H.V.M. Hamelers, Energy efficiency of a concentration gradient flow battery at elevated temperatures, *J. Power Sources* 340 (2017) 71–79, <http://dx.doi.org/10.1016/j.jpowsour.2016.11.043>.
- [14] R.S. Kingsbury, O. Coronell, Osmotic ballasts enhance faradaic efficiency in closed-loop, membrane-based energy systems, *Environ. Sci. Technol.* 51 (2017) 1910–1917, <http://dx.doi.org/10.1021/acs.est.6b03720>.
- [15] E. Güler, W. van Baak, M. Saakes, K. Nijmeijer, Monovalent-ion-selective membranes for reverse electro dialysis, *J. Membr. Sci.* 455 (2014) 254–270, <http://dx.doi.org/10.1016/j.memsci.2013.12.054>.
- [16] D.A. Vermaas, J. Veerman, M. Saakes, K. Nijmeijer, Influence of multivalent ions on renewable energy generation in reverse electro dialysis, *Energy Environ. Sci.* 7 (2014) 1434–1445, <http://dx.doi.org/10.1039/C3EE43501F>.
- [17] X. Zhu, W. He, B.E. Logan, Influence of solution concentration and salt types on the performance of reverse electro dialysis cells, *J. Membr. Sci.* 494 (2015) 154–160, <http://dx.doi.org/10.1016/j.memsci.2015.07.053>.
- [18] G.M. Geise, H.J. Cassidy, D.R. Paul, E. Logan, M.A. Hickner, Specific ion effects on membrane potential and the permselectivity of ion exchange membranes, *Phys. Chem. Chem. Phys.* 16 (2014) 21673–21681, <http://dx.doi.org/10.1039/C4CP03076A>.
- [19] J.W. Post, H.V.M. Hamelers, C.J.N. Buisman, Influence of multivalent ions on power production from mixing salt and fresh water with a reverse electro dialysis system, *J. Membr. Sci.* 330 (2009) 65–72, <http://dx.doi.org/10.1016/j.memsci.2008.12.042>.
- [20] J.G. Hong, W. Zhang, J. Luo, Y. Chen, Modeling of power generation from the mixing of simulated saline and freshwater with a reverse electro dialysis system: the effect of monovalent and multivalent ions, *Appl. Energy* 110 (2013) 244–251, <http://dx.doi.org/10.1016/j.apenergy.2013.04.015>.
- [21] D.A. Vermaas, D. Kunteng, J. Veerman, M. Saakes, K. Nijmeijer, Periodic feedwater reversal and air sparging as antifouling strategies in reverse electro dialysis, *Environ. Sci. Technol.* 48 (2014) 3065–3073, <http://dx.doi.org/10.1021/es4045456>.
- [22] D.A. Vermaas, D. Kunteng, M. Saakes, K. Nijmeijer, Fouling in reverse electro dialysis under natural conditions, *Water Res.* 47 (2013) 1289–1298, <http://dx.doi.org/10.1016/j.watres.2012.11.053>.
- [23] E. Fontananova, D. Messana, R.A. Tufa, I. Nicotera, V. Kosma, E. Curcio, W. van Baak, E. Drioli, G. Di Profio, Effect of solution concentration and composition on the electrochemical properties of ion exchange membranes for energy conversion, *J. Power Sources* 340 (2017) 282–293, <http://dx.doi.org/10.1016/j.jpowsour.2016.11.075>.
- [24] A.H. Avci, P. Sarkar, R.A. Tufa, D. Messana, P. Argurio, E. Fontananova, G. Di Profio, E. Curcio, Effect of Mg²⁺ ions on energy generation by reverse electro dialysis, *J. Membr. Sci.* 520 (2016) 499–506, <http://dx.doi.org/10.1016/j.memsci.2016.08.007>.
- [25] J.G. Hong, W. Zhang, J. Luo, Y. Chen, Corrigendum to “Modeling of power generation from the mixing of simulated saline and freshwater with a reverse electro dialysis system: The effect of monovalent and multivalent ions” [*Appl. Energy* 110 (2013) 244–251], *Appl. Energy* 129 (2014) 398–399, <http://dx.doi.org/10.1016/j.apenergy.2014.05.051>.
- [26] M. Tedesco, C. Scalici, D. Vaccari, A. Cipollina, A. Tamburini, G. Micale, Towards 1kW power production in a reverse electro dialysis pilot plant with saline waters and concentrated brines, *J. Membr. Sci.* 500 (2016) 33–45, <http://dx.doi.org/10.1016/j.memsci.2015.10.057>.
- [27] S. Pawlowski, C.F. Galinha, J.G. Crespo, S. Velizarov, 2D fluorescence spectroscopy for monitoring ion-exchange membrane based technologies – reverse electro dialysis (RED), *Water Res.* 88 (2016) 184–198, <http://dx.doi.org/10.1016/j.watres.2015.10.010>.
- [28] S. Mikhaylin, L. Bazinet, Fouling on ion-exchange membranes: classification, characterization and strategies of prevention and control, *Adv. Colloid Interface Sci.* 229 (2016) 34–56, <http://dx.doi.org/10.1016/j.cis.2015.12.006>.
- [29] H.J. Lee, J.H. Choi, J. Cho, S.H. Moon, Characterization of anion exchange membranes fouled with humate during electro dialysis, *J. Membr. Sci.* 203 (2002) 115–126, [http://dx.doi.org/10.1016/S0376-7388\(01\)00792-X](http://dx.doi.org/10.1016/S0376-7388(01)00792-X).
- [30] H.J. Lee, D.H. Kim, J. Cho, S.H. Moon, Characterization of anion exchange membranes with natural organic matter (NOM) during electro dialysis, *Desalination* 151 (2003) 43–52, [http://dx.doi.org/10.1016/S0011-9164\(02\)00971-2](http://dx.doi.org/10.1016/S0011-9164(02)00971-2).
- [31] D.H. Kim, S.M. Moon, J. Cho, Investigation of the adsorption and transport of natural organic matter (NOM) in ion-exchange membranes, *Desalination* 151 (2003) 11–20, [http://dx.doi.org/10.1016/S0011-9164\(02\)00968-2](http://dx.doi.org/10.1016/S0011-9164(02)00968-2).
- [32] E. Korngold, E. Korngold, F. de Körösy, R. Rahav, M.F. Taboch, Fouling of anion-selective membranes in electro dialysis, *Desalination* 8 (1970) 195–220, [http://dx.doi.org/10.1016/S0011-9164\(00\)80230-1](http://dx.doi.org/10.1016/S0011-9164(00)80230-1).
- [33] J. Veerman, M. Saakes, S.J. Metz, G.J. Harmsen, Reverse electro dialysis: evaluation of suitable electrode systems, *J. Appl. Electrochem.* 40 (2010) 1461–1474, <http://dx.doi.org/10.1007/s10800-010-0124-8>.
- [34] F. Liu, O. Coronell, D.F. Call, Electricity generation using continuously recirculated

- flow electrodes in reverse electrodialysis, *J. Power Sources* 355 (2017) 206–210, <http://dx.doi.org/10.1016/j.jpowsour.2017.04.061>.
- [35] J.W. Post, H.V.M. Hamelers, C.J.N. Buisman, Energy recovery from controlled mixing salt and fresh water with a reverse electrodialysis system, *Environ. Sci. Technol.* 42 (2008) 5785–5790.
- [36] D.A. Vermaas, J. Veerman, N.Y. Yip, M. Elimelech, M. Saakes, K. Nijmeijer, High efficiency in energy generation from salinity gradients with reverse electrodialysis, *ACS Sustain. Chem. Eng.* 1 (2013) 1295–1302.
- [37] P. Długolecki, A. Gambier, K. Nijmeijer, M. Wessling, Practical potential of reverse electrodialysis as process for sustainable energy generation, *Environ. Sci. Technol.* 43 (2009) 6888–6894.
- [38] W. Stumm, J.J. Morgan (Eds.), *Aquatic Chemistry: Chemical Equilibria and Rates in Natural Waters*, 3rd ed., Wiley Interscience, New York, 1999, [http://dx.doi.org/10.1016/S0016-7037\(97\)81133-7](http://dx.doi.org/10.1016/S0016-7037(97)81133-7).
- [39] Metcalf & Eddy, Inc., G. Tchobanoglous, H.D. Stensel, R. Tsuchihashi, F. Burton, *Wastewater Engineering Treatment and Resource Recovery*, 5th ed., Mc-Graw Hill Education, 1994.
- [40] L.W. Little, J.C.I. Lamb, L.F. Horney, *Characterization and Treatment of Brine Wastewaters from the Cucumber Pickle Industry*, UNC Wastewater Research Center, 1976.
- [41] R Core Team, *R: A Language and Environment for Statistical Computing*, R Foundation for Statistical Computing, Vienna, Austria, 2016 <http://www.R-project.org/>.
- [42] J. Veerman, M. Saakes, S.J. Metz, G.J. Harmsen, Reverse electrodialysis: performance of a stack with 50 cells on the mixing of sea and river water, *J. Membr. Sci.* 327 (2009) 136–144, <http://dx.doi.org/10.1016/j.memsci.2008.11.015>.
- [43] N.Y. Yip, D.A. Vermaas, K. Nijmeijer, M. Elimelech, Thermodynamic, energy efficiency, and power density analysis of reverse electrodialysis power generation with natural salinity gradients, *Environ. Sci. Technol.* 48 (2014) 4925–4936, <http://dx.doi.org/10.1021/es5005413>.
- [44] F. Helfferich, *Ion Exchange*, McGraw-Hill, New York, 1962.
- [45] E. Güler, R. Elizen, D.A. Vermaas, M. Saakes, K. Nijmeijer, Performance-determining membrane properties in reverse electrodialysis, *J. Membr. Sci.* 446 (2013) 266–276, <http://dx.doi.org/10.1016/j.memsci.2013.06.045>.
- [46] G.M. Geise, B.D. Freeman, D.R. Paul, Sodium chloride diffusion in sulfonated polymers for membrane applications, *J. Membr. Sci.* 427 (2013) 186–196, <http://dx.doi.org/10.1016/j.memsci.2012.09.029>.
- [47] K.H. Mistry, H.A. Hunter, J.H. Lienhard V, Effect of composition and nonideal solution behavior on desalination calculations for mixed electrolyte solutions with comparison to seawater, *Desalination* 318 (2013) 34–47, <http://dx.doi.org/10.1016/j.desal.2013.03.015>.
- [48] A.M. Lopez, H. Dunsworth, J.A. Hestekin, Reduction of the shadow spacer effect using reverse electrodeionization and its applications in water recycling for hydraulic fracturing operations, *Sep. Purif. Technol.* 162 (2016) 84–90, <http://dx.doi.org/10.1016/j.seppur.2016.02.020>.
- [49] M. Vanoppen, A.F.A.M. Bakelants, D. Gaublomme, K.V.K.M. Schoutteten, J. Vanden Bussche, L. Vanhaecke, A.R.D. Verliefde, Properties governing the transport of trace organic contaminants through ion-exchange membranes, *Environ. Sci. Technol.* 49 (2015) 489–497, <http://dx.doi.org/10.1021/es504389q>.
- [50] D.A. Vermaas, M. Saakes, K. Nijmeijer, Doubled power density from salinity gradients at reduced intermembrane distance, *Environ. Sci. Technol.* 45 (2011) 7089–7095.
- [51] B.J. Feinberg, G.Z. Ramon, E.M.V. Hoek, Scale-up characteristics of membrane-based salinity-gradient power production, *J. Membr. Sci.* 476 (2015) 311–320, <http://dx.doi.org/10.1016/j.memsci.2014.10.023>.
- [52] N. Tanaka, M. Nagase, M. Higa, Organic fouling behavior of commercially available hydrocarbon-based anion-exchange membranes by various organic-fouling substances, *Desalination* 296 (2012) 81–86, <http://dx.doi.org/10.1016/j.desal.2012.04.010>.
- [53] R.A. Robinson, R.H. Stokes, *Electrolyte Solutions*, Second Revised edition, Butterworths, London, 1968.
- [54] H.J. Cassidy, E.C. Cimino, M. Kumar, M.A. Hickner, Specific ion effects on the permselectivity of sulfonated poly(ether sulfone) cation exchange membranes, *J. Membr. Sci.* 508 (2016) 146–152, <http://dx.doi.org/10.1016/j.memsci.2016.02.048>.
- [55] A.H. Galama, D.A. Vermaas, J. Veerman, M. Saakes, H.H.M. Rijnaarts, J.W. Post, K. Nijmeijer, Membrane resistance: the effect of salinity gradients over a cation exchange membrane, *J. Membr. Sci.* 467 (2014) 279–291, <http://dx.doi.org/10.1016/j.memsci.2014.05.046>.